Clim. Past Discuss., 8, 215–262, 2012
www.clim-past-discuss.net/8/215/2012/
doi:10.5194/cpd-8-215-2012

Climate of the Past Discussions

Little Ice Age climate and oceanic conditions of the Ross Sea, Antarctica from a coastal ice core record

R. H. Rhodes[1,2,*], N. A. N. Bertler[1,2], J. A. Baker[3], H. C. Steen-Larsen[4], S. B. Sneed[5], U. Morgenstern[2], and S. J. Johnsen[4]

[1]Antarctic Research Centre, Victoria University of Wellington, P.O. Box 600, Wellington, 6140, New Zealand
[2]GNS Science, National Ice Core Research Laboratory, P.O. Box 30-368, Lower Hutt, 5040, New Zealand
[3]School of Geography, Environment and Earth Sciences, Victoria University of Wellington, P.O. Box 600, Wellington, New Zealand
[4]Centre for Ice and Climate, Niels Bohr Institute, Juliane Maries Vej 30, 2100 Copenhagen, Denmark
[5]Climate Change Institute, University of Maine, Orono, ME 04469, USA
[*]Present address: College of Earth, Ocean and Atmospheric Sciences, Oregon State University, Corvallis, OR 97331, USA

Received: 29 November 2011 – Accepted: 13 December 2011 – Published: 10 January 2012

Correspondence to: R. H. Rhodes (rachael.rhodes@geo.oregonstate.edu)

CPD
8, 215–262, 2012

Abstract

The Little Ice Age (LIA) is the most recent abrupt climate change event. Understanding its forcings and associated climate system feedbacks is made difficult by a scarcity of Southern Hemisphere paleoclimate records. In this paper we utilise ice core glaciochemical records to reconstruct atmospheric and oceanic conditions in the Ross Sea sector of Antarctic, a region influenced by two contrasting meteorological regimes: katabatic winds and cyclones. Stable isotope (δD) and lithophile element concentration (e.g., Al) records indicate that the region experienced ~1.75 °C cooler temperatures and strong (>57 m s^{-1}) prevailing katabatic winds during the LIA. We observe that the 1590–1875 record is characterised by high d-excess values and marine element (e.g., Na) concentrations, which are linked to the intrusion of cyclonic systems. The strongest katabatic wind events of the LIA, marked by Al, Ti and Pb concentration increases of an order of magnitude (>120 ppb Al), also occur during this interval. Furthermore, concentrations of the biogenic sulphur species MS$^-$ suggest that biological productivity in the Ross Sea Polynya was ~80 % higher prior to 1875 than in the subsequent time. We propose that colder temperatures and intensified cyclonic activity in the Ross Sea promoted stronger katabatic winds across the Ross Ice Shelf, resulting in an enlarged polynya with increased sea ice and bottom water production. It is therefore hypothesised that increased bottom water formation during the LIA occurred in response to atmospheric circulation change.

1 Introduction

The Little Ice Age (LIA) terminated only ca. 150 yr ago and is the most recent of several cooling events that punctuated the Holocene (Domack and Mayewski, 1999; Masson et al., 2000). The cause of the LIA has been widely speculated upon (e.g. Ammann et al., 2007; Broecker, 2000; Crowley, 2000), but no consensus has been reached, despite the multitude of meteorological instrumental and proxy records available from

CPD
8, 215–262, 2012

the Northern Hemisphere (Jones et al., 2009). In particular, it is unclear what role the thermohaline circulation of the world's oceans may have played in instigating or amplifying the climate response (Broecker, 2000). The timing, magnitude and character of the LIA climate response varies regionally (Matthews and Briffa, 2005), so an important aspect to understanding this event is the interpretation of Southern Hemisphere records of paleoclimate, but few are currently available (Jones and Mann, 2004).

Antarctic ice cores are valuable archives of past climate and several ice cores have recently been obtained with sufficient temporal resolution to record the LIA. Whilst significant spatial and temporal variability exists (Masson et al., 2000; Morgan and van Ommen, 1997; Mosley-Thompson and Thompson, 1990; Stenni et al., 2002), records suggest that Antarctica experienced cooling synchronous with the Northern Hemisphere during the LIA (Bertler et al., 2011) – an observation that is not consistent with the standard bi-polar seesaw model of oceanic thermohaline circulation reorganisation as the driver of climatic change (Broecker, 2000).

In this study, we examine the climate of the LIA in a key region of Antarctica using sub-annual resolution glaciochemical records from a coastal ice core retrieved from Mt. Erebus Saddle (MES), close to the edge of the Ross Ice Shelf in the Southwestern Ross Sea sector (Fig. 1). The Ross Sea Polynya, which is located along the edge of the Ross Ice Shelf, is a major site of Southern Ocean sea ice generation (Tamura et al., 2008), which drives bottom water formation (Jacobs and Giulivi, 1998). Additionally, the region is the most biologically productive area of the Southern Ocean (Arrigo and van Dijken, 2003a). Consequently, climatic changes occurring here have the potential to produce feedbacks which influence both regional conditions and the global climate system (Mayewski et al., 2009). The MES ice core site is at a boundary between the influence of two contrasting meteorological regimes. Air masses originate from both the Southern Ocean, in the form of cyclones (Sinclair et al., 2010), and the interior of Antarctica, in the form of katabatic flow (Sinclair et al., 2010; Bromwich et al., 1992). The two dominant air masses have contrasting geochemical characteristics that allow them to be identified (Bertler et al., 2004b). Thus, the location of the MES ice core site

CPD
8, 215–262, 2012

allows the meteorological regimes of the interior of Antarctica and the Ross Sea region to be traced back through time in the same ice core record.

A 678 yr continuous record of ice core lithophile element concentrations from this site is shown to provide a proxy for katabatic wind speeds, which were stronger prior to 1850 than at any ensuing time. Furthermore, by linking the katabatic wind proxy with d-excess, which is associated with the incursion of marine air masses, and methylsulphonate (MS^-), a tracer of marine primary productivity, we demonstrate that stronger katabatic winds caused a larger or more persistent Ross Sea Polynya between 1590 and 1875.

2 Methodology

2.1 Study site

MES is a local snow accumulation zone situated between Mt. Erebus and Mt. Terra Nova on Ross Island at an altitude of 1600 m (Fig. 1) (77°30.90′ S, 167°40.59′ E). Ice flows from the saddle towards NNW and SSE directions. Ground penetrating radar reconnaissance indicated a depth to bedrock of 220 m and imaged parallel isochrones, suggesting favourable glaciological conditions for the preservation of a continuous, annually-resolved ice core record. A 168 m deep ice core was drilled in the central zone of minimum ice flow in December 2006. Annual temperature at the site, ascertained from firn temperature logging, is −25.6 °C. The depth-density profile generated from density measurements conducted in the field is well explained by the densification model of Herron and Langway (1980) using a critical density of 550 kg m^{-3} and an initial density of 370 kg m^{-3}. The accumulation rate, calculated from the annual layer count, is 0.22 m (H_2O equiv.) yr^{-1}.

CPD
8, 215–262, 2012

2.2 Core processing

Here we present data from the uppermost 120 m of the MES ice core, which was processed for chemical analysis using a continuous-melter-discrete sampling system (Osterberg et al., 2006) at the New Zealand Ice Core Laboratory, GNS Science. Samples obtained from the pristine interior of the core were suitable for analysis by ion chromatography (IC) and inductively coupled plasma mass spectrometry (ICP-MS). Stable isotope ratios (δ^{18}O and δD) were determined on samples from corresponding depths obtained from the outer section of core. Between the top of the core and 66 m depth the mean sampling resolution was 43 samples m^{-1} and between 66 and 120 m depth the mean sampling resolution was increased to 61 samples m^{-1}. To improve processing efficiency an alteration to the continuous-melter-discrete sampling system enabled material for ICP-MS to be sampled at half the depth resolution (30.5 samples m^{-1}) between 77 and 120 m.

All vials used to sample material intended for IC or ICP-MS analysis were rigorously cleaned to prevent chemical contamination. The polypropylene vials used for IC samples were triple-rinsed with ultra-pure water (>18.2 MΩ), soaked for three days and triple-rinsed again. The polypropylene vials used for ICP-MS samples were first triple-rinsed with ultra-pure water then soaked in 5 wt. % analytical reagent grade HNO_3 for a minimum of 10 days, triple-rinsed, soaked in ultra-pure water for a minimum of 3 days and triple-rinsed with ultra-pure water.

Procedural blanks were used to monitor the potential contribution of the processing and sampling procedures to the concentrations of chemical species measured, and were generated from mock ice cores of frozen ultra-pure water (>18.2 MΩ), which were processed, melted and sampled daily by the methods described above. The chemical concentrations recorded in the procedural blanks (Table 1) are negligible compared to the variability in concentration exhibited in the ice core record. The significant concentrations of Ca and Zr recorded in the procedural blanks originate from ceramic

CPD
8, 215–262, 2012

knives used to prepare the ice core for melting and therefore these elements were not considered during interpretation.

2.3 Analytical methods

2.3.1 Stable isotope ratios

The stable isotope ratios $\delta^{18}O$ and δD (where $\delta^{18}O=([(^{18}O/^{16}O)_{sample}/(^{18}O/^{16}O)_{V\text{-}SMOW}]-1)\cdot 1000$ and $\delta D=([(^{2}H/^{1}H)_{sample}/(^{2}H/^{1}H)_{V\text{-}SMOW}]-1)\cdot 1000$) were measured at the Stable Isotope Laboratory, GNS Science. Samples from the first 91 m depth of ice core were analysed with a GVI Isoprime mass spectrometer by methods reported previously (Bertler et al., 2011). The analytical precision on this instrument was ±0.1 ‰ for $\delta^{18}O$ and ±1.0 ‰ for δD, resulting in an uncertainty of ±1.3 ‰ on the second order parameter deuterium excess (d-excess = $\delta D - 8\cdot\delta^{18}O$, Dansgaard, 1964).

Samples from 92 to 120 m depth (1329–1628) were analysed using a Los Gatos Research Liquid-Water Isotope Analyser which simultaneously measures $\delta^{18}O$ and δD by laser absorption spectroscopy. $\delta^{18}O$ and δD were reported with respect to V-SMOW and normalised to internal standards: INS9 with reported values of −17.4 ‰ for $\delta^{18}O$ and, −131.0 ‰ for δD, and INS11 with reported values of −0.4 ‰ for $\delta^{18}O$ and, −4.6 ‰ for δD. The analytical precision on this instrument was ±0.2 ‰ for $\delta^{18}O$ and ±0.6 ‰ for δD, resulting in an uncertainty of ±1.7 ‰ on d-excess.

Comparison of stable isotope ratios of a batch of samples measured by mass spectrometery and by laser spectroscopy identified a systematic offset between the values determined by the two techniques. The stable isotope ratios of MES ice core samples measured by laser spectroscopy were therefore corrected for this offset. Details of this correction are provided in Appendix A. A revised analytical uncertainty for d-excess, which takes into account the errors on both instruments, is calculated as ±2.1 ‰.

CPD
8, 215–262, 2012

2.3.2 Ion chromatographic analysis of major ions

Ion chromatography analysis for major ions (Na^+, Mg^{2+}, Ca^{2+}, MS^-, Cl^-, NO_3^-, SO_4^{2-}) was conducted at the Climate Change Institute, University of Maine. Anions were measured using a Dionex AS-18 column, 400 µl sample loop with a KOH eluent concentration of 35 mM. Cations were measured using a Dionex CS-12A column and a 500 µl loop with 25 mM methanesulphonic acid eluent. Calibration using five standards bracketing the anticipated concentration range routinely achieved correlation coefficients of $R^2 > 0.99$ for all analytes. An external reference material ION-92 (Environment Canada) was analysed at dilutions of 100 and 1000 times to verify the calibration. Na^+, Mg^{2+}, Ca^{2+}, MS^-, Cl^- and SO_4^{2-} measurements are accurate to within 5 %. The reproducibility, calculated as 2·RSD (relative standard deviation) of Na^+, Mg^{2+}, Ca^{2+} and MS^- measurements is <11 % and <4 % for Cl^- and SO_4^{2-}. NO_3^- is not detectable in ION-92.

2.3.3 Inductively coupled plasma mass spectrometric analysis of trace elements

Ice core samples were analysed for concentrations of major, minor and trace elements (Na, Mg, Al, Ca, Ti, V, Mn, As, Rb, Sr, Y, Zr, Cs, Ba, La, Ce, Pr, Tl, Pb, Bi, Th, U) by ICP-MS (Agilent 7500cs Series) in the Geochemistry Laboratory of the School of Geography, Environment and Earth Sciences, Victoria University of Wellington. The operating conditions adopted for ICP-MS analysis are displayed in Table 2. An ASX-520 micro-volume autosampler linked to the ICP-MS introduced sample to the PFA Teflon nebuliser (0.2 ml min^{-1} flow rate) via a peristaltic pump. The formation of oxides in the plasma was monitored by aspirating a 1 ppb solution of Ce and tuning parameters were adjusted to maintain the proportion of the ^{140}Ce converted to $^{140}Ce^{16}O$ at <2 %. The sampling and skimmer cones were cleaned, and the sample introduction system was circulated with 5 wt. % HNO_3 (Seastar) for 1 h prior to each analytical session to reduce any possible memory effect from the samples of previous users.

CPD
8, 215–262, 2012

Calibration standards were gravimetrically diluted daily from stock standards made up from mono-elemental 1000 ppm standards. The element concentrations in the calibration standards varied according to the relative concentrations expected in the ice core samples. Additional tuning was required to calibrate measurements conducted by the two different detector types (pulse and analog) on elements which recorded $>1\,000\,000$ counts s^{-1} (Na, Mg and Al).

Samples were stored frozen prior to analysis, then thawed, and acidified to 1 wt. % HNO_3 with 68 wt. % HNO_3(Seastar) at least 12 h prior to analysis. Counts recorded on 1 wt. % HNO_3 blanks were subtracted from those recorded on samples and standards to correct for background. Detection limits are calculated as 3σ on the blank measurements (Table 1). The calibration standards were run as bracketing standards every 12 samples to correct for instrumental drift. An external reference material, SLRS-4 (National Research Council, Canada), was run at 10 times dilution during each analytical session to test the accuracy and reproducibility of the measurements (Table 3).

2.3.4 Tritium analysis

Six ice core samples from a depth range of 11 to 21.3 m were measured directly without prior tritium enrichment by ultra-low-level liquid scintillation spectrometry (Quantulus™) in a monitored tritium-free environment. The water samples were purified in a vacuum distillation system to exclude tritium contamination. Details of the tritium analysis procedure are described in Morgenstern and Taylor (2009).

3 Dating

The MES ice core was dated by annual layer counting of stable isotopic and chemical concentration signals, using key reference horizons as age tie points. A glacial flow model was used to constrain the age model below the depth of the final age tie point.

CPD
8, 215–262, 2012

3.1 Annual layer counting

A snow pit sampled at MES 2 yr prior to drilling of the ice core was dated by identifying annual peaks in $\delta^{18}O$ for the time period 2000 to 2005 (Rhodes et al., 2009). The equivalent section of the $\delta^{18}O$ record was located in the ice core to facilitate dating of the uppermost section. The annual signals of $\delta^{18}O$ and δD were well-preserved in the top 25 m of the ice core and maximum values were identified as mid-summer (1 January). NO_3^- displayed a well-defined annual signal with maximum values in winter-spring, possibly the result of production in stratospheric clouds (Michalski et al., 2005).

Molecular diffusion in the firn pore space resulted in significant smoothing of the annual $\delta^{18}O$ and δD cycles deeper down the core (Johnsen, 1977; Johnsen et al., 2000). The $\delta^{18}O$ and δD time series were therefore deconvolved/back-diffused to obtain the original high frequency signal (Johnsen, 1977; Johnsen et al., 2000). The back-diffused time series of $\delta^{18}O$ and δD were used to identify annual layers in the ice core to 90 m depth (1643).

3.2 Age tie points

A peak in levels of the radioactive hydrogen isotope tritium (^3H), related to thermonuclear bomb testing, provides an age tie point for the age model. Elevated tritium contents were determined in the MES ice core between 1964 and 1972, in line with tritium contents measured in snow pits on the Ross Ice Shelf and at Halley Bay, Antarctic Peninsula, and in New Zealand precipitation (Fig. 2). MES tritium contents are lower than those of the other Antarctic locations plotted but are similar to those measured on Law Dome material (unpublished data, not shown). This may be the result of the strong marine cyclonic influence at both MES (Sinclair et al., 2010) and Law Dome (McMorrow et al., 2002), which dilutes the stratospheric tritium signal. The initial annual layer was not adjusted to fit to this age tie point.

Positive identification of volcanic nss (non-sea salt) SO_4^{2-} deposition in the MES ice core for dating purposes (e.g., Traufetter et al., 2004) is challenging because the

CPD
8, 215–262, 2012

nssSO_4^{2-} signal is dominated by biogenic nssSO_4^{2-} from the seasonally open ocean. As an alternative, we examined the deposition history of heavy, volatile trace elements, which are emitted by volcanoes (Hinkley et al., 1994) and may be deposited on ice sheets (Kaspari et al., 2007; Kellerhals et al., 2010). In the MES ice core, Pb, Bi and Tl are all strongly enriched relative to terrestrial element concentrations in at least 8 consecutive samples between 60.5 and 61.1 m depth (Fig. 3a). The initial annual layer count suggested that this signal could be deposition from the eruption of Mt. Tambora, Indonesia in April 1815 (Simkin and Siebert, 1994). However, Vallelonga et al. (2003) attributed elevated Pb and Bi concentrations in a Law Dome ice core (Fig. 1a) at this time to emissions from Mt. Erebus, on the basis of Pb isotopic signatures. As MES is located adjacent to Mt. Erebus it is plausible that the trace element record of the MES ice core may record the eruption history of Mt. Erebus rather than that of global-scale stratospheric eruptions. In order to test this hypothesis, trace element ratios measured across the Pb, Tl and Bi peaks were compared to trace element ratios measured in the plume of Mt. Erebus (Fig. 3b). None of the trace element ratios exhibit any marked deviation from the median value of the ice core record (green line) during the proposed Mt. Tambora eruption. This lends support to attribution of the Bi, Pb and Tl peaks at 61.1 m to the Mt. Tambora eruption. Moreover, the median values (Fig. 3b, green line) of the trace element ratios across the MES ice core record are different from those of the Mt. Erebus plume (Fig. 3b, purple line) providing evidence that the ice core trace element budget is predominantly influenced by input from other sources.

Further support for the accuracy of the age model can be drawn from comparison of Pb concentrations determined in the MES ice core with the history of anthropogenic Pb contamination recorded in a high resolution ice core from Law Dome (Fig. 4). A rise in Pb/Al is seen at 1893, within 5 yr of the increase in Pb concentrations at Law Dome, which is attributed to anthropogenic activity (Vallelonga et al., 2002).

CPD
8, 215–262, 2012

3.3 Glacial flow model and dating uncertainty

The glacial flow model of Dansgaard and Johnsen (1969), tuned to the Mt. Tambora age tie point (1816, 61.1 m), defined the depth-age relationship below this depth. For comparison, annual layer counting was continued until 90 m depth, after which it became challenging to identify annual layers. The age difference between the annual layer count and the glacial flow model at 90 m is 4 yr. Although these dating methods are not independent, this difference provides an estimate of the cumulative dating error at 90 m depth. The offset between the age suggested by the initial annual layer count and the date of deposition from Mt. Tambora was 8 yr. As the initial layer count did not need to be adjusted to match the ^{3}H marker age tie point, dating is accurate to within ±1 yr between 2006 and 1964.

4 Results

4.1 Stable isotopes

δD and δ^{18}O records of the MES ice core display well-developed seasonal cycles (Fig. 5, δD shown). δD varies between a mean summer (1 January, fixed by dating) maximum of −198 ‰ and a mean winter (1 July) minimum of −224 ‰ in the 1970–2006 time period (Fig. 5). The δD and d-excess time series show different interannual variability (Fig. 6) and regression of their annual mean or maximum values produces no significant correlation.

In the long term record of MES ice core δD the only deviations below the 1950–2006 mean value of >4 yr duration occur prior to 1850 (Fig. 7). The most notable of these low δD periods are 1368–1417, 1565–1600, 1650–1682, 1752–1763 and 1831–1843. The mean δD of the pre-1850 period is 7.0 ‰ lower than that of the post-1850 record (Table 4). In contrast, the d-excess record of the MES ice core is dominated by an abrupt shift towards a consistently elevated d-excess state at 1590.

CPD
8, 215–262, 2012

The mean d-excess value of the 1590–1875 time period is 5.2 ‰ higher than that of the preceeding time period (1329–1590) and 1.3 ‰ higher than the following time period (Table 4). Between 1590 and 1875 the d-excess 5 yr running mean only deviates below the 1950–2006 mean once, at ca. 1795.

4.2 Major ion and trace element chemistry

A Pearson's correlation shows the degree of co-variability between the concentrations of the elements determined by ICP-MS (Tables 5 and 6). Na, Mg and Sr are highly correlated ($R^2 > 0.86$, $p < 0.01$) in the MES ice core record. Concentration ratios of these elements correspond to the seawater concentration ratios, indicating a marine source. In the following, we focus on the Na record but consideration of the Mg or Sr record would produce similar results. Annual maximum Na concentrations (92 ppb mean) generally occur in summer, coincident with the annual peaks in δD (Fig. 5). The Na record exhibits significant interannual variability (Fig. 6) and concentrations range from 2 to 506 ppb in the 1950–2006 record (Table 4). Over the past 678 yr, Na concentrations remained relatively constant with no abrupt changes (Fig. 7). However, the mean Na concentration increased by 9 % (Table 4) after the abrupt positive shift in d-excess observed at 1590.

Al, Ti, Mn, Rb, Y, La and Ce concentrations all inter-correlate at $R^2 > 0.5$ ($p < 0.01$) and display similar temporal variability between 1970 and 2006 (Fig. 6). This group of elements is hereafter referred to as "lithophile elements". Pb is only weakly correlated ($R^2 < 0.2$) with the lithophile elements because substantial anthropogenic input occurs during the time period considered (Fig. 4). Cs, Pr, Tl, Bi, Th and U were excluded from the correlation because they frequently were below the ICP-MS detection limit.

Concentrations of lithophile elements peak during autumn and winter months (Fig. 5, Al and Mn shown), the opposite signal to the seasonal cycles of marine elements and δD. The Al mean seasonal cycle of 1970–2006 shows a 45 % higher concentration in winter relative to summer. However, the records show significant interannual variability

CPD
8, 215–262, 2012

in timing and magnitude of inputs (Fig. 6), and concentrations range between <0.1 and 7 ppb (Table 4).

Lithophile element concentrations were significantly higher prior to 1850 compared to post-1850 (Fig. 7); the mean concentrations of Al, Mn and Ce are all >60 % higher (Table 4). Furthermore, significant variability between the behaviour of different lithophile elements, not observable in the record of the last 35 yr (Fig. 6), can be discerned in the long term record (Fig. 7). For example, the mean Ce concentrations decreased by 74 % after 1850 whilst mean Mn concentration decreased by only 38 %. The lithophile elements can be categorised by the extent of inter-correlation in the pre-1850 period (Table 6). Three discrete groups are identifiable: R^2 values of >0.52 are produced between Al, Ti and Pb, $R^2 > 0.63$ between Mn and Rb, and $R^2 > 0.92$ between Y, La, and Ce. Figures 6 and 7 both display the concentration record of one element from each of these groups.

Methylsulphonate concentrations in the MES ice core are available for the section of record dating from 1797 to 2006 and vary between 1 and 187 ppb about a mean of 54 ppb (Fig. 8). A period of significantly higher concentrations is identifiable between 1825 and 1875. The mean concentration of this period is 81 % higher than that recorded between 1876 and 2006.

5 Discussion

5.1 Climate proxies

Stable isotopic ratios (δD and δ^{18}O) in ice cores are well-established proxies of air temperature (Craig, 1961; Dansgaard, 1964). However, for the MES ice core record direct calibration of the stable isotopic paleothermometer is challenging because the effects of the extreme topography of Ross Island are not well represented in gridded reanalysis datasets and weather conditions at MES are significantly different to those of nearby weather stations.

CPD
8, 215–262, 2012

To interpret the marine chemistry record it is necessary to examine the source(s) of the aerosol and transport mechanism(s) involved. Marine aerosol may be produced by either bubble bursting over the open ocean or sourced from salts (principally mirabalite $Na_2SO_4 \cdot 10H_2O$) deposited as frost flowers that are entrained from the sea ice surface. These two mechanisms result in aerosol with differing Na^+/SO_4^{2-} values. The Na^+/SO_4^{2-} of MES ice core samples is consistently lower than that of seawater (Fig. 9). This confirms that marine aerosol at MES is sourced from open water rather than frost flowers, which would result in SO_4^{2-} depletion relative to Na^+ (Rankin et al., 2004). The timing of marine aerosol deposition during the summer months (Fig. 5) of minimum sea ice extent is also suggestive of an open water source. Additionally, there is evidence that Na is entrained from the open water of the Ross Sea Polynya. During 2002/2003, Na concentrations are anomalously low (<20 ppb) (Fig. 6, second area of green shading) and this can be attributed to the severely reduced area of the Ross Sea Polynya in the summer of this year when large icebergs prevented sea ice breakout (Arrigo and van Dijken, 2003b; Rhodes et al., 2009).

Na and d-excess show similar interannual trends in the 1970–2006 record. 90 % of d-excess peaks greater than the long term mean have corresponding peaks in Na (Fig. 6, grey shaded bars). Furthermore, the maximum summer values of Na and d-excess between 1970 and 2006 are significantly correlated ($R^2 = 0.58$, $p < 0.01$) suggesting a common source. Deuterium excess is thought to be controlled by conditions at the moisture source, which are principally relative humidity, sea surface temperature (SST) and wind speed (Merlivat and Jouzel, 1979; Petit et al., 1991), but is also controlled by the degree of super-saturation during snow flake formation and is therefore related to cloud temperature (Jouzel and Merlivat, 1984). As a result, detailed delineation of potential oceanic moisture source regions, coupled with isotopic modeling, is required to thoroughly understand the origin of the MES d-excess signal. However, we have established that more positive d-excess values are associated with inputs of marine aerosol sourced from open water. Therefore, we speculate that high d-excess values are related to increased cyclonic activity in the Ross Sea region, which

CPD
8, 215–262, 2012

promotes marine aerosol generation by bubble bursting (Kreutz et al., 2000). In support of this, back-trajectory analysis conducted for an ice core site close to the Byrd Glacier (Fig. 1b) found a statistically significant positive relationship between d-excess and the frequency of oceanic cyclone systems (Markle, 2011).

Lithophile element concentrations reflect the level of mineral dust present in ice core samples (Petit et al., 1981). With several areas of outcropping rock located within 160 km of MES in the Dry Valleys and along the Transantarctic Mountains (Fig. 1), it can be assumed that the variability of lithophile element concentrations in the MES ice core is primarily controlled by input from these, local (100s of km distance away), rather than global (1000s of km distance away), dust sources (Ayling and McGowan, 2006; Dunbar et al., 2009). We do not attempt to relate the lithophile element signatures recorded in the ice core to the various dust lithologies of the region as previous work has shown this does not provide a reliable indicator of provenance (Rhodes et al., 2011). Rather, the lack of perfect positive correlation between Al, Ti, Mn, Rb, Y, La and Ce is likely to reflect mineral-specific differential rates of weathering and transport efficiency (Caquineau et al., 1998; Reimann and De Caritat, 2000), and incongruent leaching of trace elements from mineral dusts in acidified samples (Rhodes et al., 2011).

Increased lithophile element concentrations during the autumn and winter months (Fig. 5) indicate that strong (>35 m s^{-1} at Scott Base, data available at www.cliflo.niwa.co.nz) katabatic winds originating from the continental interior are required to transport additional local mineral dust material to MES. It is also important to note that the opposite seasonal cycle of lithophile and marine element concentrations at MES (Fig. 5) supports the assignment of two different meteorological systems, katabatic winds and marine cyclones, respectively, as transport mechanisms for these chemical species.

To further investigate the relationship between the concentrations of lithophile elements measured in the MES ice core and katabatic winds, we correlate the ice core data with NCEP/NCAR reanalysis meridional wind strength (Kalnay et al., 1996). In this region of Antarctica, the meridional (south to north) component of the wind field is

CPD
8, 215–262, 2012

an approximation of katabatic wind flow (Fig. 10). No significant correlation between wind speed and lithophile element concentration could be achieved for the entire time period for which reliable Antarctic NCEP/NCAR data are available (1979–2006). However, when individual decades are studied, a significant correlation with the MES Al concentration is observed for the 1990–2000 time period (Fig. 10). In contrast to the 1980s, the 1990s were characterised by a relatively strong teleconnection between the El Nio Southern Oscillation and Antarctica (Fogt and Bromwich, 2006). This led to enhanced katabatic flow speeds in the Ross Sea region (Bertler et al., 2004a), and a stronger signal in the MES katabatic wind proxy. The area of significant correlation includes the Transantarctic Mountains to the south of MES, a source region for katabatic winds to the site, which further confirms katabatic flow as the mechanism for mineral dust transport to MES.

5.2 Little Ice Age climate

The LIA record captured in the MES ice core (1329–1850) is characterised by elevated lithophile element concentrations (Fig. 7, Table 4). The rapid decrease in lithophile element concentrations between 1850 and 1853 therefore suggests the LIA ceased at this time. The ice core record dates back to 1329 and there is no significant change in the record to indicate that the onset of the LIA is captured. A frequently cited date for the onset of the LIA in the Northern Hemisphere is 1450 (Grove, 1988) but estimates vary; an ice core record from the Antarctic Dry Valleys (Bertler et al., 2011), and a tree ring climate reconstruction from South America (Villalba, 1994) have suggested the onset was ca. 150 yr earlier in the Southern Hemisphere.

As lithophile element concentrations in the MES ice core record are proxies for katabatic wind strength, the elevated concentrations suggest greater katabatic wind activity during the LIA. Formulating an approximation of how much stronger katabatic winds were is challenging, principally because the relationship between dust entrainment and wind speed is not linear (Bagnold, 1941; Pye, 1987; Schulz et al., 1998). However, as the elevated lithophile element concentrations of the LIA are not repeated

CPD
8, 215–262, 2012

in the post-1850 ice core record, we can assume that wind speeds did not reach such strength again. At Scott Base the maximum daily gust speed recorded since 1972 was 57.7 m s^{-1} from due south, so we conclude that LIA maximum wind speeds must have exceeded this value.

By examining the behaviour of the three groups of lithophile elements identified in Sect. 4.2 and their links to mineralogy and wind speed, considerable climate variability within the LIA is revealed. Al, Ti and Pb show increased mean concentrations (Table 4) coupled with discrete periods of dramatic concentration increases of several orders of magnitude during the LIA (Fig. 7). These elements are predominantly sourced from complex silicate minerals, such as feldspars, which have relatively high densities and are resistant to mechanical weathering meaning their grain size remains relatively large. High density and grain size of particles increases the threshold wind velocity for transport in suspension (Bagnold, 1941). The discrete periods of increased Al, Ti and Pb concentrations therefore represent the most extreme wind speeds of the LIA period. In contrast, the lithophile elements of the second group, Mn and Rb, which show relatively muted concentration increases during the LIA, are common in Fe-Mn oxyhydroxides and sheet silicate minerals, such as clays and micas, respectively. All of these minerals have relatively low densities and are easily weathered, forming flake-like particles of a low, uniform grain size. As a result a lower threshold wind velocity is required to initate transport of these minerals in suspension (Bagnold, 1941). It can therefore be assumed that Mn and Rb concentrations in the MES ice core do not reflect maximum wind strength in the LIA. The third group of lithophile elements, consisting of La, Ce and Y, show characteristics of both the other two groups. During discrete time periods of the LIA, concentrations increase by an order of magnitude but the timings of these extreme events do not always match that of the greatest increases in Al and Ti (Fig. 7). Similarly to Mn, La, Ce and Y are abundant in ferromanganese oxyhydroxide minerals but they are also common impurities in apatite.

The MES δD record suggests that colder temperatures, as well as stronger winds, than those experienced in the past 50 yr prevailed during the LIA. The significant

CPD
8, 215–262, 2012

deviations in δD below the 1950 to 2006 mean identified in Sect. 4.1 all date from the LIA. Additionally, sustained cold temperatures appear to be linked to the strongest katabatic flow events as the three most recent cold periods identified in the MES ice core (1650–1682, 1752–1763 and 1831–1843) occur synchronously with the strongest wind events of the LIA, as recorded by the concentrations of Al (Fig. 7), Ti and Pb. In the absence of representative weather station data with which to calculate a local δ – temperature slope, we employ the Taylor Dome δ – borehole temperature calibration of 4 ‰ δD/°C (Steig et al., 1998) to estimate the degree of cooling experienced at MES during the LIA. Taylor Dome is also located in the Ross Sea region (Fig. 1a) and is the most proximal ice core for which a local δ – temperature slope has been established. The difference between the mean δD of the LIA and the post-LIA period is 7 ‰ (Table 4), which equates to a mean cooling of 1.75 °C during the LIA. This estimate agrees with the ~2 °C cooling reported for this time period at Victoria Lower Glacier in the Northern McMurdo Dry Valleys (Fig. 1c) (Bertler et al., 2011).

Furthermore, the transition towards higher values of d-excess, which occurs at 1590 and the effects of which persist until 1875, coupled with an accompanying increase in mean Na concentration, suggests that the intrusion of marine cyclones was more frequent during this time. This may be linked to findings of Kreutz et al. (2000) who used the Siple Dome Na record as a sea level pressure proxy and identified an alteration in periodicity at ca. 1600 linked to deepening of the principal low pressure system off West Antarctica.

5.3 Ross Sea Polynya in the Little Ice Age

Although the MS^- record of the MES ice core has limited temporal coverage it provides a proxy record of Ross Sea Polynya area (Rhodes et al., 2009). The higher concentrations recorded between 1825 and 1875 indicate that the polynya area was greater during this time. As variability in katabatic wind strength has been directly linked to polynya size (Morales Maqueda et al., 2004), we conclude that the stronger katabatic winds of the Little Ice Age caused this change in polynya size. Increased polynya

CPD
8, 215–262, 2012

area exerts a positive feedback on marine primary productivity (Arrigo and van Dijken, 2004). By extrapolating the linear relationship between MS^{-} concentration (x) and primary production rate (y) established by Rhodes et al. (2009) ($y = 1.35x - 3.41$), we calculate that between 1825 and 1875 primary productivity rates were approximately 80 % higher than the post-1875 level.

Diatom abundances from two sediment cores taken west of Ross Island reveal a period of increased primary productivity between 1825 and 1880 (Leventer and Dunbar, 1988). This timing closely corresponds to the interval of higher MS^{-} concentrations observable in the MES record (Fig. 8). A further, more prolonged, time period (1600–1875) of increased open water diatom populations is identified in a four sediment cores retrieved from the north and northwest of Ross Island (Leventer and Dunbar, 1988). Taking into account dating errors, this corresponds remarkably well to the period of high d-excess values recorded in the MES ice core (1590–1875) (Fig. 7).

Greater polynya extent and primary productivity appear to be linked to the increased cyclonic activity identified in the MES ice core. For the katabatic winds that maintain the polynya to propagate across the relatively flat Ross Ice Shelf a strong pressure gradient is required and this is created by the presence of cyclonic systems (Bromwich et al., 1993, 1992). We propose that the combination of colder temperatures and increased cyclonic activity in the Ross Sea region led to stronger katabatic flows which maintained a spatially larger and/or more temporally persistent polynya between 1590 and 1875. Supporting evidence for stronger katabatic winds across East Antarctica during this interval of the LIA is found in an ice core micro-particle record from South Pole (Mosley-Thompson, 1995).

In addition, we consider the possibility that greater polynya size in the LIA led to increased rates of sea ice production, which amplified Antarctic Bottom Water formation in the Ross Sea. Furthermore, it is conceivable that the increased katabatic wind strength recorded in the MES and South Pole ice cores affected the other wind-driven polynyas around the Antarctic continent (Morales Maqueda et al., 2004). Increased bottom water formation in Antarctic coastal polynyas may be the source of the increase

CPD
8, 215–262, 2012

in Southern Hemisphere bottom water formation during in the LIA identified by Broecker et al. (1999). In combination with enhanced primary productivity, this would have resulted in increased drawdown of atmospheric CO_2 into the ocean, contributing to the 6–8 ppm decrease in atmospheric CO_2 concentration observed in other Antarctic ice cores between ca. 1600 and 1800 (Etheridge et al., 1996; Indermuhle et al., 1999).

6 Conclusions

Stable isotope, major ion and trace element chemistry records from the MES ice core document the last 678 yr of climate in the Southwestern Ross Sea region of Antarctica at sub-annual resolution. Dating of the record is accomplished by a combination of annual layer counting and a glacial flow model, with the timing of anthropogenic Pb deposition in Antarctica providing support for accuracy of the age model. Examination of the monthly resolution record of the last 35 yr allowed climate proxies to be developed. Lithophile elements concentrations are controlled by mineral dust transport by katabatic winds whilst d-excess and marine element concentrations are related to incursion of marine cyclones.

The MES ice core record suggests that the Ross Sea region experienced colder temperatures (by ~1.75 °C) and strong (>57 m s^{-1}) katabatic winds during the LIA. A decrease in lithophile elements concentrations between 1850 and 1853 indicates a substantial reduction in katabatic wind strength and marks the termination of the LIA. Furthermore, the d-excess and Na records provide evidence for a more frequent incursion of marine cyclones into the Ross Sea between 1590 and 1875. The ice core MS^{-} record and diatom blooms recorded in sediment cores (Leventer and Dunbar, 1988) indicate that marine primary productivity was increased during this time, indicating that polynya area was greater. Colder temperatures and increased cyclonic activity promoted stronger katabatic winds across the Ross Ice Shelf, causing sea ice divergence and creating a greater polynya area in the Ross Sea.

CPD
8, 215–262, 2012

We hypothesize that increased sea ice formation resulting from greater polynya extent caused increased rates of bottom water formation at this time. Change in the thermohaline circulation of the oceans could therefore be a response to, rather than the initial driver of, climate change at the LIA.

Appendix A

Comparison between mass spectrometer and laser spectroscopy δD and δ^{18}O measurements

To test the comparability of measurements conducted by mass spectrometer and by laser spectroscopy a batch of samples ($n = 187$) was analysed by both instruments. Comparison of the stable isotope ratios measured on the two instruments identified offsets between the datasets, most notably for δD (Fig. A1). The offsets between the δD and δ^{18}O values produced a significant offset between the calculated values of d-excess (Fig. A2). For several samples tested, the difference between the d-excess derived from the GVI mass spectrometer and that derived from the LGR Liquid-Water Isotope Analyser data is greater than the analytical uncertainty. Therefore, the δD and δ^{18}O values measured on the LGR Liquid-Water Isotope Analyser (δD_{laser}) were corrected to make them comparable to the GVI mass spectrometer values ($\delta D_{mass\,spec.\,equiv.}$) using the linear relationships established by analysing samples on both instruments (e.g. Fig. A1).

$$\delta D_{mass\,spec.\,equiv.} = \delta D_{laser}/0.9809 + 1.6576$$
$$\delta^{18}O_{mass\,spec.\,equiv.} = \delta^{18}O_{laser}/1.0034 - 0.1577$$

Deuterium excess values were then calculated from the corrected δD and δ^{18}O datasets. A revised analytical uncertainty (u) for d-excess, which takes into account the errors on both instruments, is calculated as: This value is applied when the entire

CPD
8, 215–262, 2012

record encompassing stable isotope ratios measured by both instruments is considered. The δD and d-excess records of the MES ice core before and after the above corrections were applied are displayed in Fig. A3.

Acknowledgements. We sincerely thank Antarctica New Zealand, the US Polar Program, and Scott Base and McMurdo Station staff for logistical support. We thank the Alfred Wegener Institute for lending us the AWI ice core drill. Recovery of this ice core was made possible by Alex Pyne, Webster Drilling, and Glenn and Tony Kingan. Ice cores were carefully transported back to Scott Base by Ken Borek Ltd. and Helicopters New Zealand. Ground penetrating radar surveys were conducted by Matt Watson, ScanTec Ltd. Thanks to the staff of the Stable Isotope Laboratory, GNS Science, for their dedication to this work. This project is funded through the Marsden Fund (VUW0509) and the New Zealand Ministry for Science and Innovation via contracts awarded to Victoria University of Wellington and GNS Science (VICX0704, CO5X0202 and CO5X0902).

References

Ammann, C. M., Joos, F., Schimel, D. S., Otto-Bliesner, B. L., and Tomas, R. A.: Solar influence on climate during the past millennium: Results from transient simulations with the NCAR Climate System Model, P. Natl. Acad. Sci., 104, 3713–3718, 2007.

Arrigo, K. R. and van Dijken, G. L.: Phytoplankton dynamics within 37 Antarctic coastal polynya systems, J. Geophys. Res., 108, 3271, doi:10.1029/2002JC001739, 2003a.

Arrigo, K. R. and van Dijken, G. L.: Impact of iceberg C-19 on Ross Sea primary production, Geophys. Res. Lett., 30, 1836, doi:10.1029/2003GL017721, 2003b.

Arrigo, K. R. and van Dijken, G. L.: Annual changes in sea-ice, chlorophyll-*a* and primary production in the Ross Sea, Antarctica, Deep-Sea Res. Pt. II, 51, 117–138, 2004.

Ayling, B. F. and McGowan, H. A.: Niveo-eolian sediment deposits in coastal South Victoria Land, Antarctica: indicators of regional variability in weather and climate, Arct. Antarct. Alpine Res., 38, 313–324, 2006.

Bagnold, R. A.: The Physics of Blown Sand and Desert Dunes, Methuen, New York, 265 pp., 1941.

CPD
8, 215–262, 2012

Bertler, N. A. N., Barrett, P. J., Mayewski, P. A., Fogt, R. L., Kreutz, K. J., and Shulmeister, J.: El Niño suppresses Antarctic warming, Geophys. Res. Lett., 31, L15207, doi:10.1029/2004GL020749, 2004a.

Bertler, N. A. N., Mayewski, P. A., Barrett, P. J., Sneed, S. B., Handley, M. J., and Kreutz, K. J.: Monsoonal circulation of the McMurdo Dry Valleys, Ross Sea Region, Antarctica: signal from the snow chemistry, Ann. Glaciol., 39, 139–145, 2004b.

Bertler, N. A. N., Mayewski, P. A., and Carter, L.: Cold conditions in Antarctica during the Little Ice Age – implications for abrupt climate change mechanisms, Earth Planet. Sc. Lett., 308, 41–51, 2011.

Broecker, W. S.: Was a change in thermohaline circulation responsible for the Little Ice Age?, P. Natl. Acad. Sci., 97, 1339–1342, 2000.

Broecker, W. S., Sutherland, S., and Peng, T.-H.: A possible 20th-century slowdown of Southern Ocean deep water formation, Science, 286, 1132–1135, 1999.

Bromwich, D. H., Carrasco, J. F., and Stearns, C. R.: Satellite observations of katabatic-wind propagation for great distances across the Ross Ice Shelf, Mon. Weather Rev., 120, 1940–1949, 1992.

Bromwich, D. H., Carrasco, J. F., Liu, Z., and Tzeng, R.: Hemispheric moisture variations and oceanographic impacts associated with katabatic surges across the Ross Ice Shelf Antarctica, J. Geophys. Res., 98, 13045–13062, 1993.

Caquineau, S., Gaudichet, A., Gomes, L., Magonthier, M., and Chatenet, B.: Saharan dust: clay ratio as a relevant tracer to assess the origin of soil-derved aerosols, Geophys. Res. Lett., 25, 983–986, 1998.

Craig, H.: Isotopic variations in meteoric waters, Science, 133, 1702–1703, 1961.

Crowley, T. J.: Causes of climate change over the past 1000 years, Science, 289, 270–277, 2000.

Dansgaard, W.: Stable isotopes in precipitation, Tellus, 16, 436–468, 1964.

Dansgaard, W. and Johnsen, S. J.: A flow model and a time scale for the ice core from Camp Century, Greenland, J. Glaciol., 8, 215–223, 1969.

Domack, E. W. and Mayewski, P. A.: Bi-polar ocean linkages: evidence from late-Holocene Antarctic marine and Greenland ice-core records, Holocene, 9, 247–251, 1999.

Dunbar, G. B., Bertler, N. A. N., and McKay, R. M.: Sediment flux through the McMurdo Ice Shelf in Windless Bight, Antarct. Global Planet. Change, 69, 87–93, 2009.

CPD
8, 215–262, 2012

Etheridge, D. M., Steele, L. P., Langenfelds, R. L., Francey, R. J., Barnola, J. M., and Morgan, V. I.: Natural and anthropogenic changes in atmospheric CO_2 over the last 1000 years from air in Antarctic ice and firn, J. Geophys. Res., 101, 4115–4128, 1996.

Fogt, R. L. and Bromwich, D. H.: Decadal variability of the ENSO teleconnection to the high-latitude South Pacific governed by coupling with the Southern Annular Mode, J. Climate, 19, 979–998, 2006.

Grove, J. M.: The Little Ice Age, Methuen, London, 1988.

Herron, M. M. and Langway, C. C.: Firn densification: An empirical model, J. Glaciol., 25, 373–385, 1980.

Hinkley, T. K., Le Cloarec, M. F., and Lambert, G.: Fractionation of families of major, minor, and trace metals across the melt-vapor interface in volcanic exhalations, Geochim. Cosmochim. Acta, 58, 3255–3263, 1994.

Indermuhle, A., Stocker, T. F., Joos, F., Fischer, H., Smith, H. J., Wahlen, M., Deck, B., Mastroianni, D., Tschumi, J., Blunier, T., Meyer, R., and Stauffer, B.: Holocene carbon-cycle dynamics based on CO_2 trapped in ice at Taylor Dome, Antarctica, Nature, 398, 121–126, 1999.

Jacobs, S. S. and Giulivi, C. F.: Interannual ocean and sea ice variability in the Ross Sea., in: Antarctic Research Series, edited by: Jacobs, S. S. and Weiss, R., AGU, Washington, DC, 135–150, 1998.

Jochum, K. P., Nohl, U., Herwig, K., Lammel, E., Stoll, B., and Hofmann, A. W.: GeoReM: a new geochemical database for reference materials and isotopic standards, Geostand. Geoanal. Res., 29, 333–338, 2005.

Johnsen, S. J.: Stable isotope homogenisation of polar firn and ice, International symposium on isotopes and impurities in snow and ice, General Assembly XVI, Washington, DC, 210–219, 1977.

Johnsen, S. J., Clausen, H. B., Cuffey, K. M., Hoffmann, G., Schwander, J., and Creyts, T.: Diffusion of stable isotopes in polar firn and ice: the isotope effect in firn diffusion, Phys. Ice Core Rec., edited by: Hondoh, T., Hokkaido University Press, Sapporo, Japan, 121–140, 2000.

Jones, P. D. and Mann, M. E.: Climate over past millennia, J. Climate, 42, RG2002, doi:10.1029/2003RG000143, 2004.

Jones, P. D., Briffa, K. R., Osborn, T. J., Lough, J. M., van Ommen, T. D., Vinther, B. M., Luterbacher, J., Wahl, E. R., Zwiers, F. W., Mann, M. E., Schmidt, G. A., Ammann, C. M., Buckley, B. M., Cobb, K. M., Esper, J., Goosse, H., Graham, N., Jansen, E., Kiefer, T., Kull, C., Küttel, M., Mosley-Thompson, E., Overpeck, J. T., Riedwyl, N., Schulz, M., Tudhope, A. W., Villalba, R., Wanner, H., Wolff, E., and Xoplaki, E.: High-resolution palaeoclimatology of the last millennium: a review of current status and future prospects, Holocene, 19, 3–49, 2009.

Jouzel, J. and Merlivat, L.: Deuterium and oxygen 18 in precipitation: Modeling of the isotopic effects during snow formation, J. Geophys. Res., 89, 11749-11757, 1984.

Kalnay, E., Kanamitsu, M., Kistler, R., Collins, W., Deaven, D., Gandin, L., Iredell, M., Saha, S., White, G., Woollen, J., Zhu, Y., Leetmaa, A., Reynolds, R., Chelliah, M., Ebisuzaki, W., Higgins, W., Janowiak, J., Mo, K. C., Ropelewski, C., Wang, J., Jenne, R., and Joseph, D.: The NCEP/NCAR reanalysis 40-year project, B. Am. Meteorol. Soc., 77, 437–471, 1996.

Kaspari, S., Mayewski, P., Kang, S., Sneed, S., Hou, S., Hooke, R., Kreutz, K., Introne, D., Handley, M., Maasch, K., Qin, D., and Ren, J.: Reduction in northward incursions of the South Asian monsoon since 1400 AD inferred from a Mt. Everest ice core, Geophys. Res. Lett., 34, L16701, doi:10.1029/2007GL030440, 2007.

Kellerhals, T., Tobler, L., Brütsch, S., Sigl, M., Wacker, L., Gäggeler, H. W., and Schwikowski, M.: Thallium as a tracer for preindustrial volcanic eruptions in an ice core record from Illimani, Bolivia, Environ. Sci. Technol., 44, 888–893, 2010.

Kreutz, K. J., Mayewski, P. A., Pittalwala, I. I., Meeker, L. D., Twickler, M. S., and Whitlow, S. I.: Sea level pressure variability in the Amundsen Sea region inferred from a West Antarctic glaciochemical record., J. Geophys. Res., 105, 4047–4059, 2000.

Leventer, A. and Dunbar, R. B.: Recent diatom record of McMurdo Sound, Antarctica: Implications for history of sea ice extent, Paleoceanography, 3, 259–274, 1988.

Markle, B. R., Bertler, N. A. N., Sinclair, K. E., and Sneed, S. B.: Synoptic variability in the Ross Sea region, Antarctica as seen from back-trajectory modeling and ice core analysis, J. Geophys. Res., doi:10.1029/2011JD016437, in press, 2011.

Masson, V., Vimeux, F., Jouzel, J., Morgan, V., Delmotte, M., Ciais, P., Hammer, C., Johnsen, S. J., Lipenkov, V. Y., Mosley-Thompson, E., Petit, J. R., Steig, E. J., Stievenard, M., and Vaikmae, R.: Holocene climate variability in Antarctica based on 11 ice-core isotopic records, Quaternary Res., 54, 348–358, 2000.

Matthews, J. A. and Briffa, K. R.: The "Little Ice Age": reevaluation of an evolving concept, Geogr. Ann. A, 87, 17–36, 2005.

CPD
8, 215–262, 2012

Mayewski, P. A., Meredith, M. P., Summerhayes, C. P., Turner, J., Worby, A., Barrett, P. J., Casassa, G., Bertler, N. A. N., Bracegirdle, T., Naveira-Garabato, A. C., Bromwich, D., Campbell, H., Hamilton, G. H., Lyons, W. B., Maasch, K. A., Aoki, S., Xiao, C., and van Ommen, T.: State of the Antarctic and Southern Ocean climate system, Rev. Geophys., 47, 1–38, 2009.

McMorrow, A., Curran, M. A. J., van Ommen, T. D., Morgan, V., and Allison, I.: Features of meteorological events preserved in a high-resolution Law Dome (East Antarctica) snow pit, Ann. Glaciol., 35, 463–470, 2002.

Merlivat, L. and Jouzel, J.: Global climatic interpretation of the deuterium-oxygen 18 relationship for precipitation, J. Geophys. Res., 84, 5029–5033, 1979.

Michalski, G., Bockheim, J. G., Kendall, C., and Thiemens, M.: Isotopic composition of Antarctic Dry Valley nitrate: implications for NO_y sources and cycling in Antarctica, Geophys. Res. Lett., 32, L13817, doi:10.1029/2004gl022121, 2005.

Morales Maqueda, M. M. A., Willmott, A. J., and Biggs, N. R. T.: Polynya dynamics: a review of observations and modeling, Rev. Geophys., 42, RG1004, doi:10.1029/2002RG000116, 2004.

Morgan, V. and van Ommen, T. D.: Seasonality in late-Holocene climate from ice-core records, Holocene, 7, 351–354, 1997.

Morgenstern, U. and Taylor, C. B.: Ultra low-level tritium measurement using electrolytic enrichment and LSC, Isot. Environ. Health S., 45, 96–117, 2009.

Mosley-Thompson, E.: Paleoenvironmental conditions in Antarctica since A.D. 1500: ice core evidence, in: Climate Since A.D. 1500, edited by: Bradley, R. S. and Jones, P. D., Routledge, 572, 1995.

Mosley-Thompson, E. and Thompson, L. G.: Little Ice Age (neoglacial) paleoenvironmental conditions at Siple Station, Antarctica, Ann. Glaciol., 14, 199–204, 1990.

Osterberg, E. C., Handley, M. J., Sneed, S. B., Mayewski, P. A., and Kreutz, K. J.: Continuous ice core melter system with discrete sampling for major ion, trace element, and stable isotope analyses, Environ. Sci. Technol., 40, 3355–3361, 2006.

Parish, T.: Surface winds over the Antarctic continent: a review, Rev. Geophys., 26, 169–180, 1988.

Petit, J. R., Briat, M., and Royer, A.: Ice age aerosol content from East Antarctic ice core samples and past wind strength, Nature, 293, 391–394, 1981.

Petit, J. R., White, J., Young, N. W., Jouzel, J., and Korotkevitch, Y. S.: Deuterium excess in Antarctic snow, J. Geophys. Res., 96, 5113–5122, 1991.

CPD
8, 215–262, 2012

Pye, K.: Aeolian Dust and Dust Deposits, Academic Press, London, 1987.
Rankin, A. M., Wolff, E. W., and Mulvaney, R.: A reinterpretation of sea-salt records in Greenland and Antarctic ice cores?, Ann. Glaciol., 39, 276–282, 2004.
Reimann, C. and De Caritat, P.: Intrinsic flaws of element enrichment factors (EFs) in environmental geochemistry, Environ. Sci. Technol., 34, 5084–5091, 2000.
Rhodes, R. H., Bertler, N. A. N., Baker, J. A., Sneed, S. B., Oerter, H., and Arrigo, K. R.: Sea ice variability and primary productivity in the Ross Sea, Antarctica, from methylsulphonate snow record, Geophys. Res. Lett., 36, L10704, doi:10.1029/2009GL037311, 2009.
Rhodes, R. H., Baker, J. A. B., Millet, M.-A., and Bertler, N. A. N.: Experimental investigation of the effects of mineral dust on the reproducibility and accuracy of ice core trace element analysis, Chem. Geol., 286, 207–221, 2011.
Schulz, M., Balkanski, Y., Guelle, W., and Dulac, F.: Role of aerosol size distribution and source location in a three-dimensional simulation of a Saharan dust episode tested against satellite derived optical thickness, J. Geophys. Res., 103, 10579-10592, 1998.
Simkin, T. and Siebert, L.: Volcanoes of the world, 2nd Edn., Geoscience Press, Tuscon, Arizona, 349 pp., 1994.
Sinclair, K. E., Bertler, N. A. N., and Trompetter, W. J.: Synoptic controls on precipitation pathways and snow delivery to high-accumulation ice core sites in the Ross Sea region, Antarctica, J. Geophys. Res., 115, D22112, doi:10.1029/2010jd014383, 2010.
Steig, E. J., Brook, E. J., White, J. W. C., Sucher, C. M., Bender, M. L., Lehman, S. J., Morse, D. L., Waddington, E. D., and Clow, G. D.: Synchronous climate changes in Antarctica and the North Atlantic, Science, 282, 92–95, 1998.
Stenni, B., Proposito, M., Gragnani, R., Flora, O., Jouzel, J., Falourd, S., and Frezzotti, M.: Eight centuries of volcanic signal and climate change at Talos Dome (East Antarctica), J. Geophys. Res., 107, 4076, doi:10.1029/2000jd000317, 2002.
Tamura, T., Ohshima, K. I., and Nihashi, S.: Mapping of sea ice production for Antarctic coastal polynyas, Geophys. Res. Lett., 35, C07030, doi:10.1029/2007GL032903, 2008.
Traufetter, F., Oerter, H., Fischer, H., Weller, R., and Miller, H.: Spatio-temporal variability in volcanic sulphate deposition over the past 2 kyr in snow pits and firn cores from Amundsenisen, Antarctica, J. Glaciol., 50, 137–146, 2004.
Vallelonga, P., Van de Velde, K., Candelone, J., Morgan, V. I., Boutron, C. F., and Rosman, K.: The lead pollution history of Law Dome, Antarctica, from isotopic measurements on ice cores: 1500 AD to 1989 AD, Earth Planet. Sc. Lett., 204, 291–306, 2002.

CPD
8, 215–262, 2012

Vallelonga, P., Candelone, J. P., Van de Velde, K., Curran, M. A. J., Morgan, V. I., and Rosman, K. J. R.: Lead, Ba and Bi in Antarctic Law Dome ice corresponding to the 1815 AD Tambora eruption: an assessment of emission sources using Pb isotopes, Earth Planet. Sc. Lett., 211, 329–341, 2003.

Villalba, R.: Tree-ring and glacial evidence for the Medieval Warm Epoch and the Little Ice Age in Southern South America, Clim. Change, 26, 183–197, 1994.

Zreda-Gostynska, G., Kyle, P. R., Finnegan, D., and Prestbo, K. M.: Volcanic gas emissions from Mount Erebus and their impact on the Antarctic environment, J. Geophys. Res., 102, 15039–15055, 1997.

CPD
8, 215–262, 2012

Table 1. Procedural blank concentrations and detection limits (3σ on blank) of elements determined by ICP-MS (ppt = parts per trillion) and major ions determined by IC (ppb = parts per billion).

Element/major ion	Procedural blank	Detection limit
Na	1120	167
Mg	290	5.02
Al	560	9.72
Ca	6890	1271
Ti	78.5	22.5
V	0.70	0.83
Mn	10.9	3.22
As	0.29	6.73
Rb	0.47	0.31
Sr	4.50	0.31
Y	0.50	0.10
Zr	3.05	0.58
Cs	0.05	0.18
Ba	5.28	0.32
La	0.66	0.14
Ce	1.42	0.19
Pr	0.17	0.19
Tl	0.00	0.44
Pb	4.67	0.72
Bi	0.09	0.43
Th	0.07	0.45
U	0.04	0.40
Na^+	0.34	0.16
Mg^{2+}	0.66	0.51
K^+	0.10	0.33
Ca^{2+}	20.3	0.08
MS^-	0.00	0.32
Cl^-	26.6	0.76
SO_4^{2-}	12.8	0.43
NO_3^-	6.27	0.35

CPD
8, 215–262, 2012

Table 2. Operating conditions of the ICP-MS and data acquisition parameters for the determination of selected elements in MES ice core samples.

Parameter	Setting
Forward power	1500 W
RF matching	1.75–1.84 V
Carrier gas	1.04–1.10 l min^{-1}
Makeup gas	0 l min^{-1}
Nebulizer pump	0.12–0.16 rps
Spray chamber temperature	2 °C
Sampling depth	7 mm
Torch position	Optimised daily to maximise sensitivity
Ion lenses voltages	Optimised daily to maximise sensitivity and signal stability across mass range
Isotopes measured	^{23}Na, ^{24}Mg, ^{27}Al, ^{43}Ca, ^{47}Ti, ^{51}V, ^{55}Mn, ^{75}As, ^{85}Rb, ^{88}Sr, ^{89}Y, ^{90}Zr, ^{133}Cs, ^{138}Ba, ^{139}La, ^{140}Ce, ^{141}Pr, ^{205}Tl, ^{208}Pb, ^{209}Bi, ^{232}Th, ^{238}U
Uptake and stabilization time	50 and 60 s
Washing time between samples	10 s H_20, 200 s 5 wt. % HNO_3 (Seastar), 220 s 1 wt. % HNO_3 (total 430 s)
Integration time	0.10 or 0.15 s depending on element
No. of runs and scan passes	3 × 26

CPD
8, 215–262, 2012

Table 3. Element concentrations (ppt) determined by repeated measurement of SLRS-4 riverine water standard ($n = 82$) with precision and accuracy of measurements.

Element	This study	Certified values	Precision 2·RSD[b] (%)	Accuracy (% difference)
Na[a]	2289 ± 80	2400 ± 200	3.5	4.6
Mg[a]	1573 ± 156	1600 ± 100	9.9	1.7
Al[a]	56 ± 4	54 ± 4	6.8	4.0
Ca[a]	6132 ± 546	6200 ± 200	8.9	1.1
Mn[a]	3.56 ± 0.14	3.37 ± 0.18	4.0	5.5
Ba[a]	13.0 ± 0.44	12.22 ± 0.6	3.4	6.4
Ti	1587 ± 152	1460 ± 80	9.6	8.7
V	382 ± 19	320 ± 30	5.1	19.3
As	757 ± 21	680 ± 60	2.7	11.3
Rb	1616 ± 59	1530 ± 50	3.7	5.6
Sr	29 783 ± 1269	26 300 ± 3200	4.3	13.2
Y	143 ± 6	146 ± 8	4.0	2.0
Zr	139 ± 45	120 ± 15	32.2	15.9
Cs	6.80 ± 0.23	9 ± 1	3.4	24.5
La	298 ± 15	287 ± 8	5.1	3.9
Ce	375 ± 27	360 ± 12	7.3	4.1
Pr	83.4 ± 10.6	69.3 ± 1.8	12.6	20.4
Tl	7.96 ± 2.31	6.8 ± 1.3	29.0	17.0
Pb	82.0 ± 5.7	86 ± 7	6.9	4.7
Bi	2.40 ± 0.34	2.1 ± 0.1	14.0	14.4
Th	21.5 ± 1.9	18 ± 3	9.1	19.6
U	51.1 ± 4.9	50 ± 3	9.6	2.3

[a] Concentrations in parts per billion (ppb).
[b] RSD = relative standard deviation.

Certified values for SLRS-4 are GeoREM (Jochum et al., 2005) preferred values obtained from http://georem.mpch-mainz.gwdg.de.

CPD
8, 215–262, 2012

Table 4. Mean and range (in parentheses) of selected stable isotopic and chemistry parameters within specified time intervals of the MES ice core record.

	δD (‰)	d-excess (‰)	Na (ppb)	Al (ppb)	Mn (ppt)	Ce (ppt)
1950–2006	−211.6	7	76.5	1.33	61.9	4.0
	(−254.1 to −130.4)	(0 to 22)	(2.15 to 506)	(0.09 to 7.06)	(0 to 301)	(0 to 24.3)
1850–2006	−209.0	8	95.7	1.64	55.7	4.1
(post-LIA)	(−255.0 to −130.4)	(0 to 22)	(2.15 to 853)	(2.02 to 18.9)	(0 to 472)	(0 to 26.6)
1329–1850	−216.0	6	91.4	4.38	94.5	17.0
(LIA)	(−269.2 to −147.3)	(−4 to 21)	(1.54 to 1170)	(0.19 to 141)	(0 to 1046)	(0.21 to 375)
1590–1875	−214.7	9	96.2	5.20	93.4	16.9
	(−269.2 to −157.5)	(1 to 21)	(1.54 to 1170)	(0.20 to 141)	(0 to 1046)	(0.10 to 374)
1329–1590	−216.7	4	87.8	3.47	91.1	15.8
	(−256.7 to −147.3)	(−4 to 14)	(4.73 to 557.6)	(0.29 to 40.9)	(2.8 to 543)	(0.6 to 362)

CPD
8, 215–262, 2012

Table 5. Correlation coefficients for major, minor and trace element concentrations (12 samples yr^{-1}) during the 1970–2006 time period in MES ice core. All values shown are significant at the 99 % level, $n = 439$.

R^2	Na	Mg	Al	Ti	V	Mn	Rb	Sr	Y	Ba	La	Ce	Pb
Na	1												
Mg	0.86	1											
Al	–	0.02	1										
Ti	–	–	0.51	1									
V	0.36	0.38	0.44	0.52	1								
Mn	–	0.02	0.75	0.55	0.39	1							
Rb	0.15	0.15	0.61	0.58	0.73	0.47	1						
Sr	0.90	0.90	0.06	0.06	0.50	0.06	0.27	1					
Y	–	–	0.42	0.43	0.29	0.44	0.46	0.02	1				
Ba	–	–	0.12	0.18	0.08	0.13	0.13	0.03	0.12	1			
La	–	–	0.75	0.69	0.53	0.62	0.71	0.05	0.52	0.10	1		
Ce	–	–	0.74	0.68	0.51	0.64	0.68	0.05	0.54	0.09	0.97	1	
Pb	–	–	0.11	0.21	0.06	0.16	0.13	0.03	0.13	0.49	0.10	0.09	1

CPD
8, 215–262, 2012

Table 6. Correlation coefficients for lithophile element concentrations (2 samples yr^{-1}) during the LIA recorded in MES ice core (1329–1850). All values shown are significant at the 99 % level, $n = 1043$.

R^2	Al	Ti	Mn	Rb	Y	La	Ce	Pb
Al	1							
Ti	0.81	1						
Mn	0.13	0.12	1					
Rb	0.07	0.06	0.63	1				
Y	0.08	0.06	0.52	0.43	1			
La	0.06	0.05	0.45	0.38	0.92	1		
Ce	0.10	0.08	0.45	0.36	0.94	0.98	1	
Pb	0.59	0.52	–	–	–	–	–	1

CPD
8, 215–262, 2012

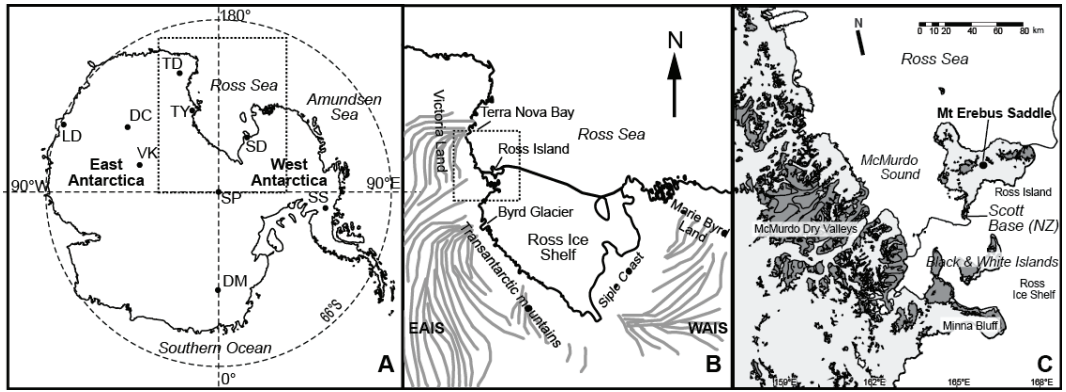

Fig. 1. (A) Map of the Antarctic continent. Locations of major ice core sites are marked by solid black circles and are labelled as follows: DC = EPICA Dome C, DM = EPICA Dronning Maud Land, LD = Law Dome, SD = Siple Dome, SP = South Pole, SS = Siple Station, TD = Talos Dome, TY = Taylor Dome. The dashed rectangle defines the area of map B. **(B)** Map of the Ross Sea region bound by the East Antarctic Ice Sheet (EAIS) and the West Antarctic Ice Sheet (WAIS). Approximate katabatic flow paths are indicated by grey arrows (modified after Parish, 1988). The dashed rectangle defines the area of map C. **(C)** Map of McMurdo Sound area. The location of Mt. Erebus Saddle (MES) is shown. Dark grey shading indicates areas of exposed rock outcrop.

CPD
8, 215–262, 2012

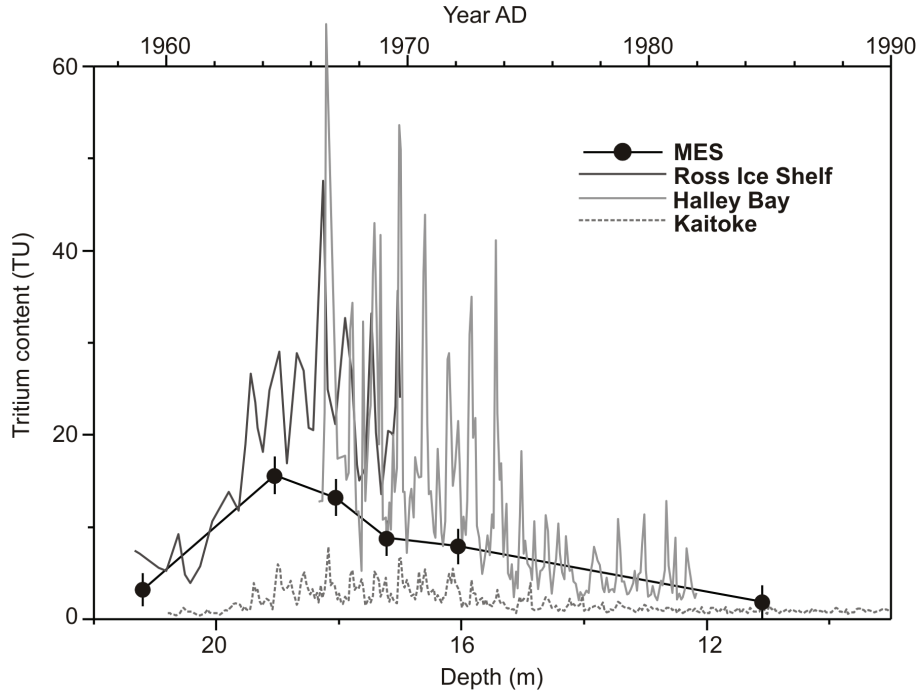

Fig. 2. Tritium contents of six MES ice core samples plotted with tritium contents of precipitation from the Ross Ice Shelf, Halley Bay, Antarctic Peninsula, and Kaitoke, New Zealand, decay-corrected to December 2006. Error bars are 1σ. The detection limit for analysis without prior enrichment is 2.5 TU. One tritium unit (TU) is defined as one atom of tritium per 10^{18} atoms of hydrogen, equivalent to 0.118 becquerels (Bq) per litre of water.

CPD
8, 215–262, 2012

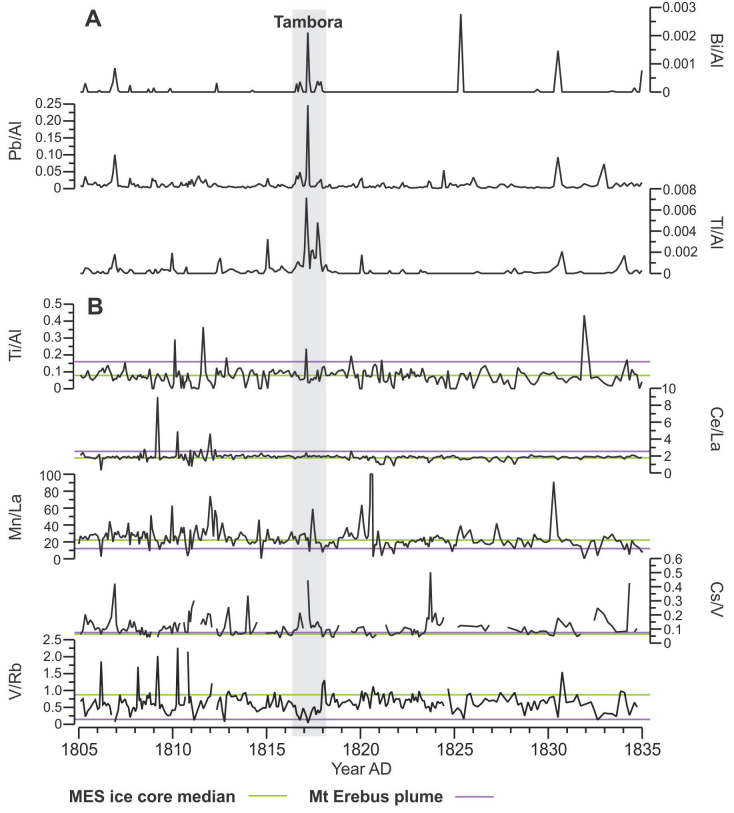

Fig. 3. (A) Bi, Pb and Tl concentrations normalised to Al (a terrestrial element) across the Mt. Tambora eruption marker (grey shading). **(B)** Trace element ratio records from the MES core for the same time period, plotted with values for the Mt. Erebus plume (purple line) (Zreda-Gostynska et al., 1997) and the median values of the entire MES ice core record (green line). Breaks in the record occur where the concentration of an element is below the ICP-MS detection limit. Information on Bi, Pb and Tl content of the Mt. Erebus plume is not available.

CPD
8, 215–262, 2012

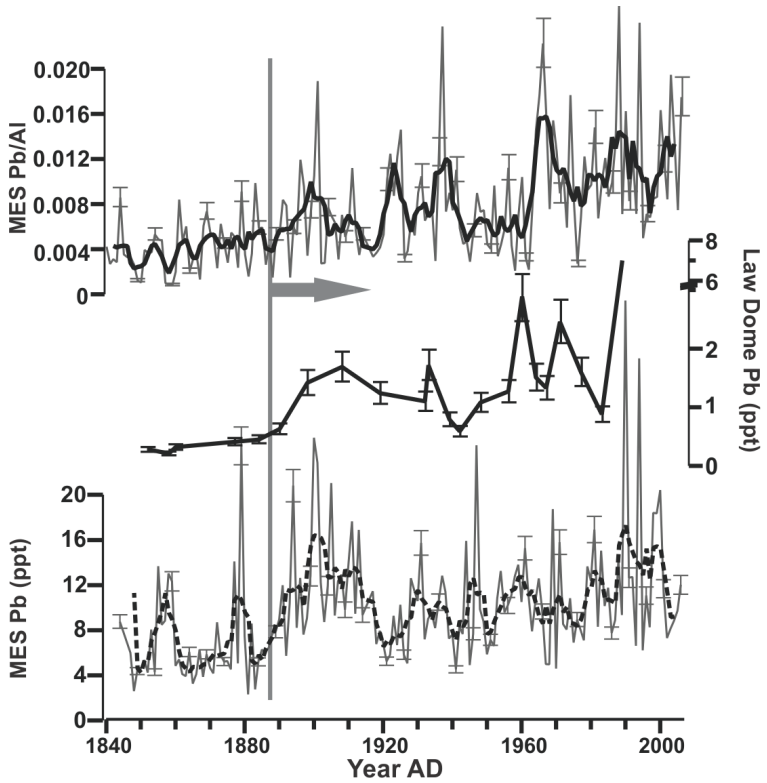

Fig. 4. Anthropogenic influence on Pb deposition at MES since 1840. All MES data plotted are annual means to remove seasonal variability. A 5 yr running mean is plotted through the MES Pb concentration data (dashed line). MES Pb concentrations are also shown normalised to Al to remove the influence of variable mineral dust contributions. Pb concentrations determined at Law Dome are plotted for comparison (Vallelonga et al., 2002). Grey arrow indicates onset of anthropogenic Pb pollution determined at Law Dome. All error bars are $\pm 2\sigma$.

CPD
8, 215–262, 2012

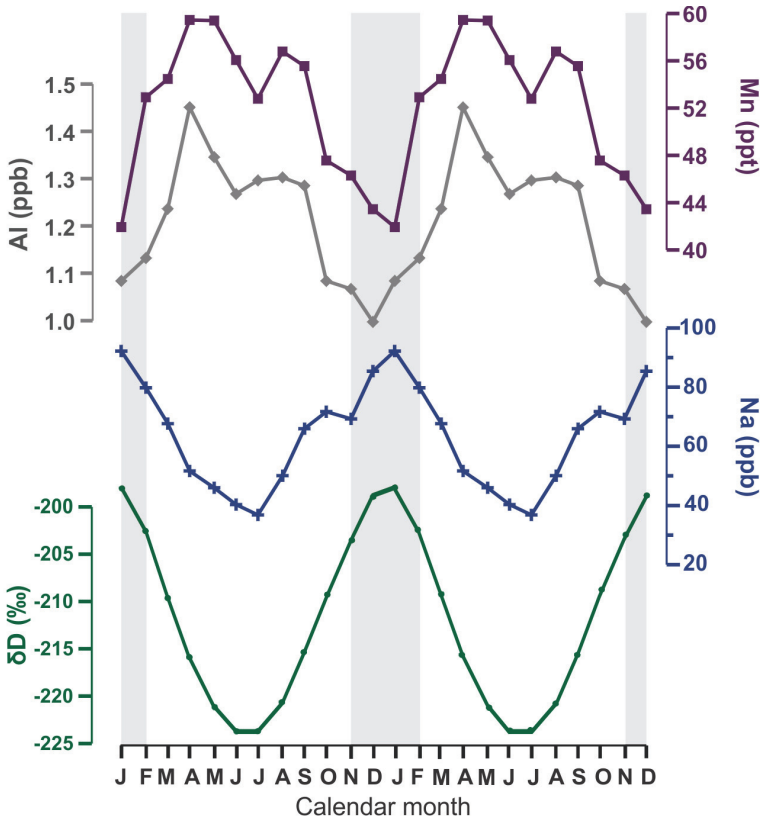

Fig. 5. Mean seasonal cycles of δD, d-excess, marine aerosol (Na) and lithophile elements (Al and Mn) for 1970–2005. Two cycles are plotted to aid viewing. δD has been back-diffused to correct for changes in amplitude and phasing of seasonal cycles resulting from molecular diffusion.

CPD
8, 215–262, 2012

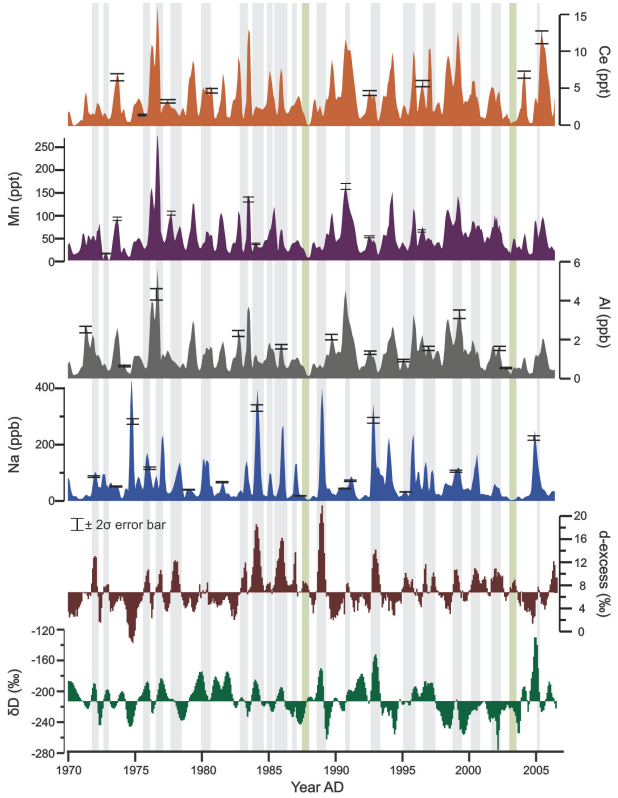

Fig. 6. Stable isotope and chemistry data for the time period 1970–2006 of the MES ice core. All the time series have been re-sampled to monthly resolution and a 3 month running mean has then been applied to the Na, Al, Mn and Ce time series. δD and d-excess are plotted around 1970–2006 mean values. Representative analytical error bars ($\pm 2\sigma$) are displayed on selected points. δD analytical error bars are too small to plot and the d-excess analytical error is indicated. Shaded bars highlight d-excess values exceeding the 1970–2006 mean with associated Na peaks (grey shading) and without associated Na peaks (green shading).

CPD
8, 215–262, 2012

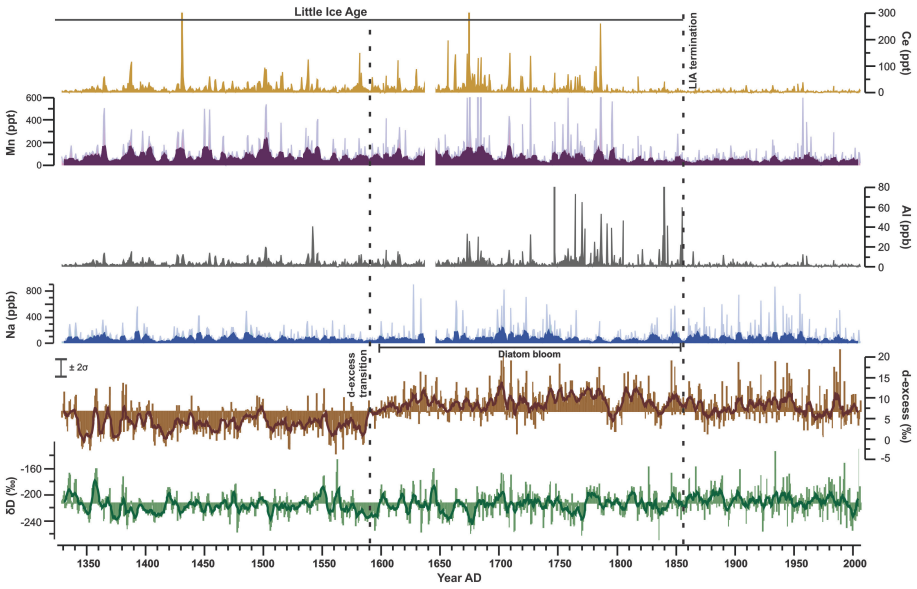

Fig. 7. Stable isotope and chemistry records from the MES ice core re-sampled to 2 samples yr^{-1}. 5 yr smoothed time series are plotted in bold colours for all time series except Al and Ce. δD and d-excess are plotted around 1950–2006 mean values. The d-excess analytical error applicable to the entire dataset is indicated. Al plot is clipped at 80 ppb and Mn plot is clipped at 600 ppt. Timing of a diatom bloom reported by Leventer and Dunbar (1988) in four sediment core records from the north-west of Ross Island in McMurdo Sound is indicated. The gap in ICP-MS data is due to the removal of anomalously high chemistry concentrations relating to a tephra layer in the ice core.

CPD
8, 215–262, 2012

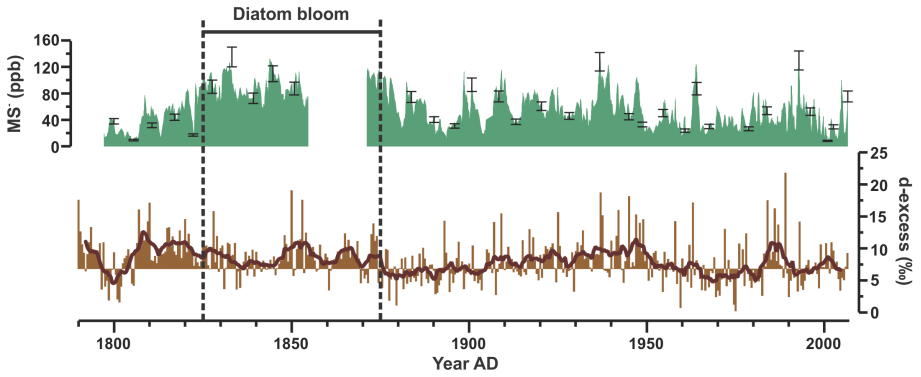

Fig. 8. Deuterium excess and MS^- time series from MES ice core. MS^- is raw data smoothed by 5-point running mean. Deuterium excess time series re-sampled to 2 samples yr^{-1} and smoothed by 5 yr running mean (as Fig. 7). Timing of a diatom bloom reported by Leventer and Dunbar (1988) in two sediment core records from McMurdo Sound, to the west of Ross Island, is indicated. Representative analytical error bars ($\pm 2\sigma$) are displayed on selected points. The gap in the MS^- time series exists because some samples have not been analysed for MS^- concentration.

CPD
8, 215–262, 2012

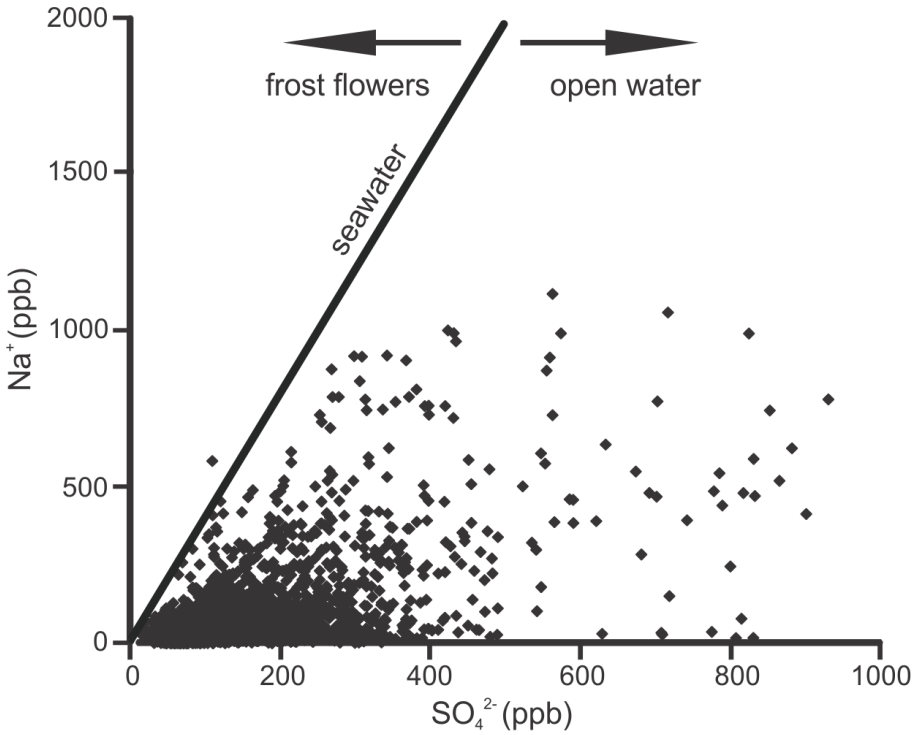

Fig. 9. Scatterplot of Na^+ versus SO_4^{2-} concentrations of all MES samples measured by IC (surface-65.8 m; 1793–2006). Black line is the Na^+/SO_4^{2-} of seawater and all samples, except one, plot below this line. Na^+/SO_4^{2-} values indicate Na^+ is sourced from the open ocean.

CPD
8, 215–262, 2012

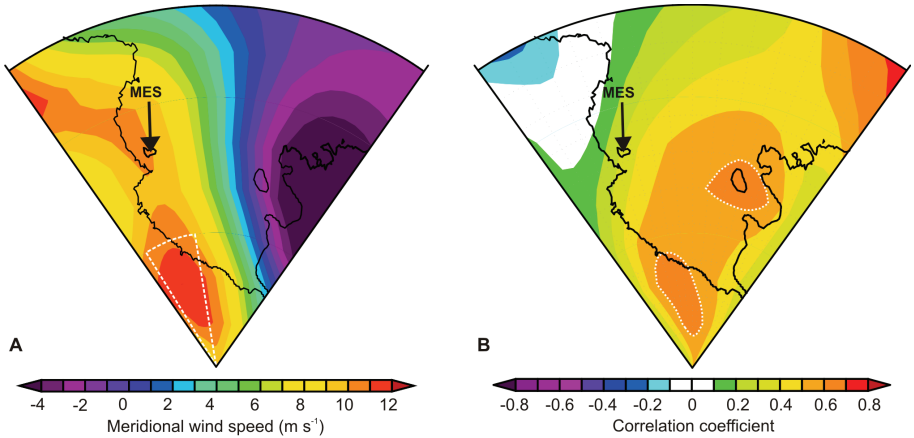

Fig. 10. (A) NCEP/NCAR reanalysis 850 mb meridional wind composite mean for the winter months (JJA) of 1979–2006 across the Ross Sea region (90–70° S, 150–220° E). White dashed line defines the source region of meridional winds arriving at MES. **(B)** Spatial correlation pattern between meridional wind (850 mb) and MES AI concentration record for the winter months (JJA) of 1990–2000 across the Ross Sea region. White dashes outline region of significant correlation ($p < 0.025$, $n = 10$).

CPD
8, 215–262, 2012

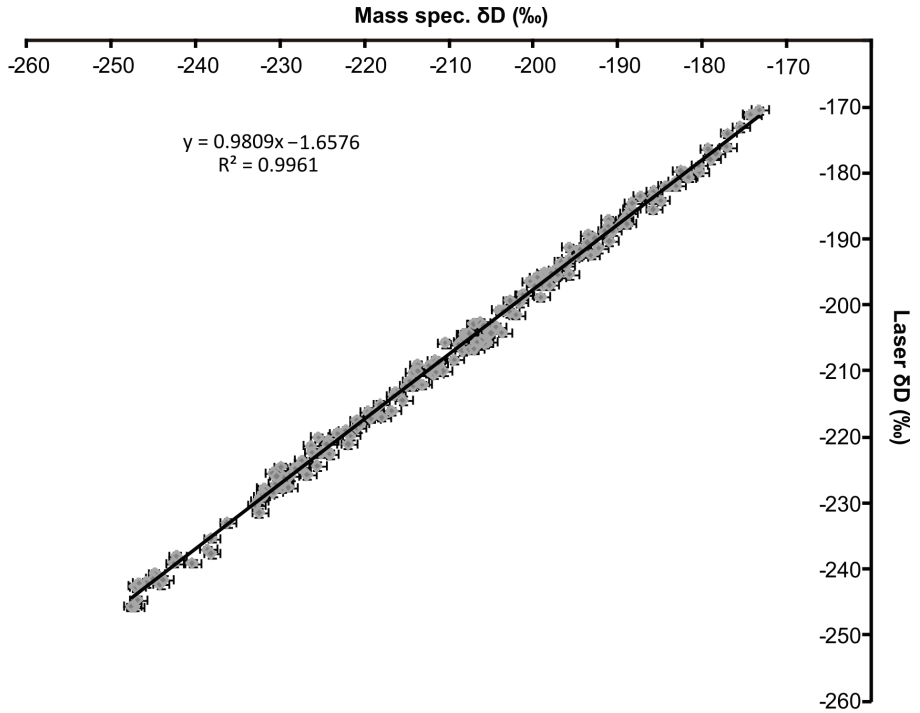

Fig. A1. δD measured on GVI mass spectrometer and LGR Liquid-Water Isotope Analyser (Laser). Error bars are 2σ.

CPD
8, 215–262, 2012

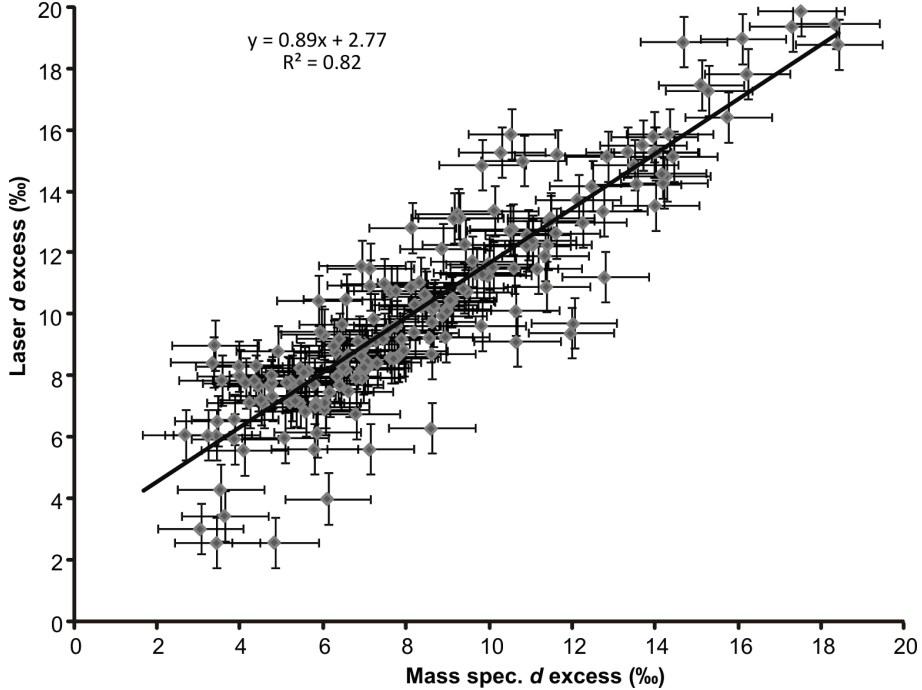

Fig. A2. Deuterium excess derived from 18O and δD values measured on GVI mass spectrometer and LGR Liquid-Water Isotope Analyser (Laser). Error bars are analytical uncertainty (u) ($u = \sqrt{(a^2 + (8 \cdot b^2))}$, where a = precision on δ^{18}O and b = precision on δD).

CPD
8, 215–262, 2012

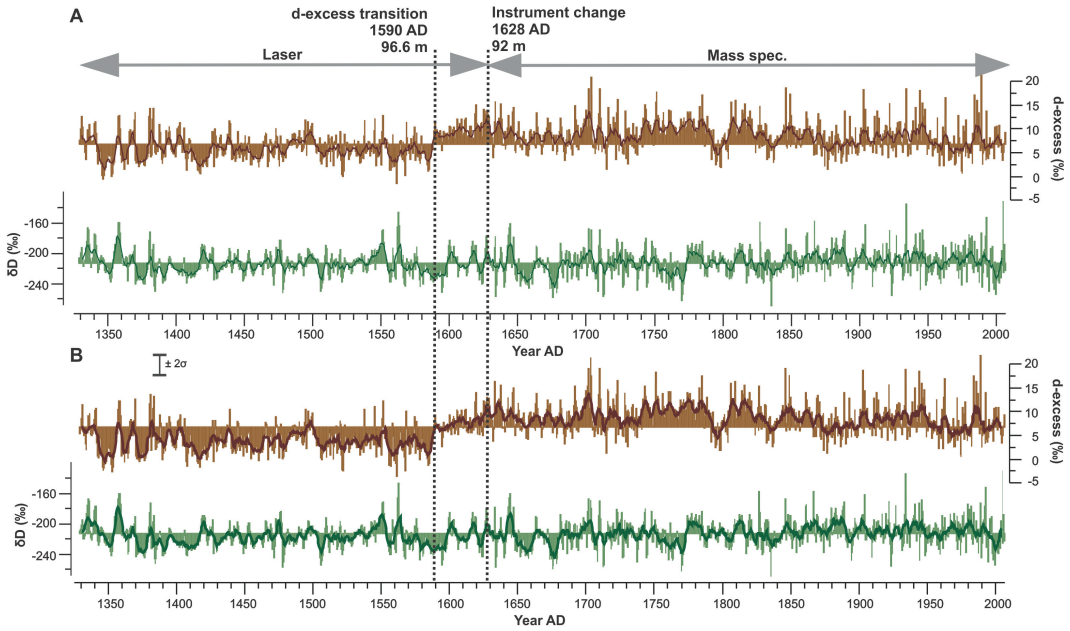

Fig. A3. Stable isotope records of the MES ice core **(A)** before, and **(B)** after, a correction was applied to laser-measured data to account for the calibration difference between the mass spectrometer and laser instruments.

CPD
8, 215–262, 2012